Modeling and Stability Analysis of a Direct-Drive Direct-Grid Slip–Synchronous Permanent-Magnet Wind Generator

Johannes H. J. Potgieter, *Student Member, IEEE*, and Maarten J. Kamper, *Senior Member, IEEE*

***Abstract*—In order to simplify and increase the reliability of wind generators, a new type of a direct-drive directly grid-connected wind generator known as a slip–synchronous permanent-magnet generator (SS-PMG) is proposed. It consists of two integrated generating units, i.e., a directly turbine-connected slip PMG unit and a directly grid-connected PM synchronous generator unit. The main aim of this paper is to determine if this generator is stable under transient wind turbine and grid conditions. A transfer function model is developed to evaluate the dynamic performance of the wind generator system. The transient response of a single 15-kW grid-connected system is evaluated. It is shown that the generator is very stable under transient turbine torque conditions. Furthermore, it acts as a filter to prevent voltage flickering due to oscillatory turbine pulsations. A very important design aspect to take into account is the torque ripple characteristics of the slip PM generator as torque ripple can be transferred to the grid current under certain conditions. Simulated and dynamically measured results are shown for a series of 15-kW SS-PMG prototypes.**

***Index Terms*—Dynamic response, permanent-magnet generator (PMG), power systems, stability, wind power generation.**

I. Introduction

MOST wind turbine generators currently installed consist of a directly grid-connected variable-speed doubly fed induction generator, with a gearbox and a partially rated power electronic converter. With gearbox failures being costly and leading to long downtimes, gearless direct-drive full-variable-speed permanent-magnet generators (PMGs) that are connected to the grid via a full-rated power electronic converter are considered in several new installations. However, due to the steep rise in the price of PM materials in recent times, synchronous generators with wound rotors and smaller medium-speed PMGs that are operated with a gearbox having a lower gearing ratio are also considered. Although not as severe as gearbox failures and with the components affected easier to replace, electrical failures are the most common type of failure for wind generator systems. Thus, it is clear that, if the gearbox and the power electronic converter are removed from the drivetrain, the reliability of wind turbine systems can be increased significantly. This means that maintenance requirements, the income loss due to downtime and, thus, the operating cost will be reduced accordingly. In particular, for systems with limited access such as offshore wind turbines where some studies suggest that the operation and maintenance costs can be more than 20% of the total cost of a wind farm, the aforementioned aspects can play a significant role.

In order to reduce the complexity of the drivetrain, there are experimental proposals in literature where a synchronous generator is directly connected to the grid. An example of such topologies is the spring and damper system proposed by Westlake *et al.* [1] to damp power angle oscillations. Research is also being conducted on the directly grid-connected synchronous generator that is operated in conjunction with a hydrodynamically coupled gearbox. The gearbox has a variable speed input and a fixed speed output at the generator side. The work done in [2] explains the modeling and the transient response of such a system. Another direct-grid PM wind generator topology reported in literature is the concept proposed in [3], where a partially rated converter is placed in the star point of the generator. Power fluctuations can be then actively damped by means of this converter.

Another much simpler directly grid-connected and direct-drive wind generator topology is the slip–synchronous PMG (SS-PMG) that has been only very recently proposed in [4]. The SS-PMG is based on the concept that was first introduced in 1926 by Punga and Schon [5], which was known as the permanent-magnet induction generator (PMIG). It was initially proposed to improve the power factor of conventional induction machines. Within the last decade, the PMIG was also suggested to be used as a gearless direct-drive utility-scale wind generator in [6] and [7]. The PMIG can be also operated as a direct-drive variable-speed doubly fed PMG with a partially rated converter, as proposed in [8]. Several other research works on the PMIG concept exist, with the contribution of each more thoroughly discussed in [4].

Many of the issues regarding the direct grid connection of the SS-PMG have been already addressed in [9]–[12]. In [9], the synchronization of the SS-PMG to the grid is discussed, and in [10], low-voltage ride through (LVRT) techniques for the SS-PMG are evaluated. The reactive power flow characteristics and the compliance of the SS-PMG with the relevant grid code

Manuscript received March 10, 2013; revised July 16, 2013; accepted August 18, 2013. Date of publication September 20, 2013; date of current version May 15, 2014. Paper 2012-EMC-105.R1, presented at the 2011 IEEE International Electric Machines and Drives Conference, Niagara Falls, ON, Canada, May 15–18, and approved for publication in the IEEE TRANSACTIONS ON INDUSTRY APPLICATIONS by the Electric Machines Committee of the IEEE Industry Applications Society.

The authors are with the Department of Electrical and Electronic Engineering, University of Stellenbosch, Stellenbosch 7602, South Africa (e-mail: kamper@sun.ac.za; jpot@sun.ac.za).

Color versions of one or more of the figures in this paper are available online at http://ieeexplore.ieee.org.

Digital Object Identifier 10.1109/TIA.2013.2283019

specifications are studied in [11] and [12]. For the reactive power control of the SS-PMG, a tap-changing transformer configuration that makes use of an electronic tap-changing scheme is proposed, which is much more reliable and efficient than conventional tap-changing transformers, as discussed in [11]. It is also known that the high-voltage dc (HVDC) transmission with a central voltage source converter (VSC) is currently gaining significant interest due to the expansion of offshore wind farms. The central VSC connects the ac wind-farm collection grid to the mainland ac grid via an HVDC link. It is proposed in [13] that the frequency and voltage of the ac collection grid side of the central VSC, which consists of several SS-PMGs in this case, be made variable, mitigating the fixed speed drawback of the SS-PMG.

Although many of the grid connection aspects of the SS-PMG have been already addressed and it has been shown that the SS-PMG is a viable wind generating alternative, the stability of this generator regarding turbine and network disturbances is still questioned. This issue has never been fully addressed and is investigated in this paper. If the SS-PMG does not offer a stable grid connection in a wind generating setup, no utility will allow the connection of such a system. The aim of this paper is to thoroughly characterize the dynamic behavior of the SS-PMG system to turbine and grid disturbances, and to torque ripple disturbances within the machine itself. The d-q modeling of this type of generator receives special attention in this paper. A 15-kW wind turbine system is used as a case study, for which simulated and dynamically measured results are presented.

II. SS-PMG Technology Evaluation

The SS-PMG consists of two integrated generating units, i.e., a slip PMG with a short-circuited rotor, which is similar to an induction-machine cage rotor directly mounted to the turbine, and a PM synchronous generator (PMSG) unit, with its stator terminals directly connected to the grid. These two units are mechanically linked via a common free-rotating PM rotor, with separate sets of magnets for each of the generating units. Fig. 1(a) and (b) shows the section diagram and an example of the SS-PMG generating system, respectively. The common PM rotor rotates at a synchronous speed in accordance with the grid frequency. The turbine-connected slip rotor rotates at a relative slip speed with regard to the PM rotor. Torque is generated between the slip rotor and the PM rotor, and counter torque is generated between the stator and the PM rotor. Thus, power transfer takes place from the turbine to the slip rotor and then via the PM rotor to the stator and the grid. The steady-state operation of the system is thoroughly discussed and analyzed in [4].

The main characteristics of the SS-PMG, as opposed to other wind generator systems, can be summarized as follows.

- With no gearbox or full-rated power electronic converter, the SS-PMG comprises an extremely simple drivetrain. The PMSG unit is similar to the PM generators typically used in the wind industry, which are considered highly reliable. Furthermore, due to the second slip PMG unit operating at a much lower relative slip speed, the SS-PMG is even more reliable than the PMSG. With the gearbox and the full-rated power electronic converter being the components mostly considered in the analysis of the reliability of a wind turbine, the SS-PMG has a major advantage in this regard.
- The SS-PMG has several favorable grid-voltage supporting capabilities. As in [2], the directly grid-connected synchronous generator can provide the highest amount of reactive power compensation with respect to other wind generator topologies currently in use.
- Due to the fixed speed drawback of the SS-PMG, it is true that, for particularly low-wind-speed sites, the SS-PMG might not be a viable alternative. However, for good wind sites, the difference in the total energy capture with fixed speed versus that of variable speed turbines is not that significant, which makes the use of the SS-PMG system more attractive. It is also possible for the SS-PMG to be operated as a variable-speed wind generator, as proposed in [8] and [13]. The viability of these system proposals, however, still requires further investigation.
- Because the SS-PMG consists of two direct-drive generators, it is a concern that this generator will be less efficient. However, conventional systems consist of either a gearbox or a converter in conjunction with a generator, or both and a generator. This means that the total efficiency is

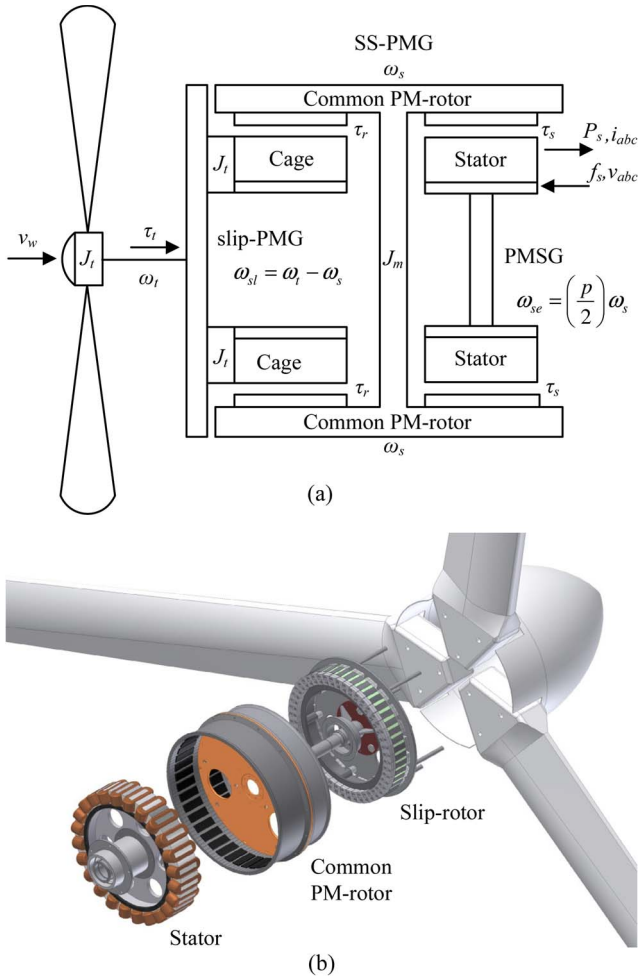

Fig. 1. (a) Cross section and (b) example of the new concept SS-PMG [4].

calculated as $\eta_{\text{total}} = \eta_{\text{gear}} \times \eta_s \times \eta_{\text{conv}}$, whereas for the SS-PMG, it is calculated as $\eta_{\text{total}} = \eta_s \times \eta_r$. (The efficiency of the PMSG unit is indicated by η_s and that of the slip PMG unit by η_r). The efficiency of the grid-connected PMSG is similar to that of the direct-drive PMGs currently in use. For the slip PMG, a value of $\eta_r = 97\%$ is shown in [14] to be easily achievable. In [4] and [14], the total system efficiency values for the SS-PMG are given in the range of $\eta_s = 91\%$–92%, which is similar to those of other wind generating systems.

- A major concern of the SS-PMG system is the increase in mass due to the addition of the second direct-drive PMG. However, in [12] and [14], it is found that the increase in the active mass and PM content is about 1.5 p.u., with 1 p.u. indicating the active mass only of the PMSG unit. The total tower top mass increase for small-scale SS-PMG systems is estimated at about 10%–20%, as in [14].
- It is also a concern that, by adding the second generator unit to the design, the complexity of the generator increases significantly. However, it should be noted that the slip rotor of the second generator is similar to a conventional aluminum cage rotor with simple construction. Furthermore, due to the low slip speed and almost zero electrical frequency, solid magnets, yokes, and conductors can be used, and very little wear can be expected on the bearings. The axial separation of the two machine units, as proposed in [4] and as shown in Fig. 1, allows for the easy assembly of the complete SS-PMG, which significantly is not more complex than the assembly of conventional PMSGs.

Thus, due to the slip PMG unit being simpler and smaller than the PMSG unit, the cost increase of adding the second generator unit is not as significant as would be expected. In the calculation of the initial component cost of the direct-drive direct-grid SS-PMG, it should be taken into account that the cost of the power electronic converter needs to be omitted. Furthermore, the cost savings incurred over the lifetime of the wind turbine due to the reduced operation and maintenance cost of the SS-PMG needs to be taken into account. Currently, the SS-PMG seems very favorable for small-scale wind generation, with attempts to commercialize this technology currently under way. Whether high-power SS-PMGs are feasible is still open to question, but studies are being currently conducted regarding the applicability of this technology for utility-scale systems.

III. Dynamic Wind Generator Aspects

To evaluate the dynamic behavior of the SS-PMG under transient torque conditions and transient grid disturbances, information on the characteristics of these disturbances is required. Furthermore, some knowledge of the relevant standards and grid codes, as in [15], is required in order to obtain an idea of what is expected of the SS-PMG system regarding its dynamic behavior when connected to the grid. In this section, the three main types of disturbances in a wind generator setup are described.

A. Turbine Transients

As explained in the literature, there are torque disturbances in a wind generator system, which could cause, among other things, serious voltage flickering. This is an important aspect in wind power generation, and its effect should be kept as low as possible. Typical methods to asses flickering are specified according to international standards and guidelines, as in the International Electrotechnical Commission (IEC) 61400-21 standard, and in general, wind generators need to comply with all the aspects within the IEC Technical Specification 61400 series. The application of this standard is thoroughly discussed in [16]. Flickering is caused by several stochastic and periodic power fluctuations prevalent in wind generator systems, as discussed in [17] and [18]. These fluctuations are mainly low frequency in nature and mostly correspond to multiples of the rotational frequency of the turbine. The rotational frequency is defined as $f_t = (n_t/60)$, where n_t is the rotational speed of the turbine in revolutions per minute. The disturbance frequency components are defined in multiples of the rotational frequency as nf_t, where n gives the harmonic order of the disturbance. The most common turbine disturbances are caused by the influence of wind shear and tower shadowing at $n = 3$, and tower oscillations at $n = 1$. Furthermore, the rapid changes in wind speed, e.g., gusts and turbulence caused by the turbine itself, and the wake effect caused by different wind turbines on one another can be causes of flickering. For a nonsite-specific modeling of the wind conditions, including turbulence intensity, the parameters in the IEC 61400-1 standard that makes use of the Kaimal spectrum, as explained in [19], can be used.

B. Generator Torque Ripple Transients

Another important factor that needs to be taken into account is the effects of the cogging torque and the load torque ripple on the system. In [20], a direct-drive PM wind generator is evaluated, where it is mentioned that the cogging torque should not be more than 1.5%–2% of the rated torque. In some studies, it is even specified to be as low as 0.5%. It is mentioned that, at very low rotational speeds, a clear resonance frequency point is prevalent. Although the resonance area is mostly below the operating speed range of the turbine, it could cause serious damage to the system if it becomes too severe as the rotor speed goes through resonance during start-up. Furthermore, under certain conditions, there are frequency components that can excite the natural frequencies of the whole turbine and tower structure, which could cause serious resonance in the physical structure and increase the fatigue loading of the system.

C. Grid Voltage Transients

As specified in all grid codes, the ability of the generator to stay connected during grid faults is of extreme importance. A typical LVRT specification is given in Fig. 2. The main issue of synchronous generators with a direct grid connection is the ability of the generators to stay in synchronism after major voltage drops [2]. Furthermore, it is stipulated in [15] that the generator needs to be able to handle frequency variations

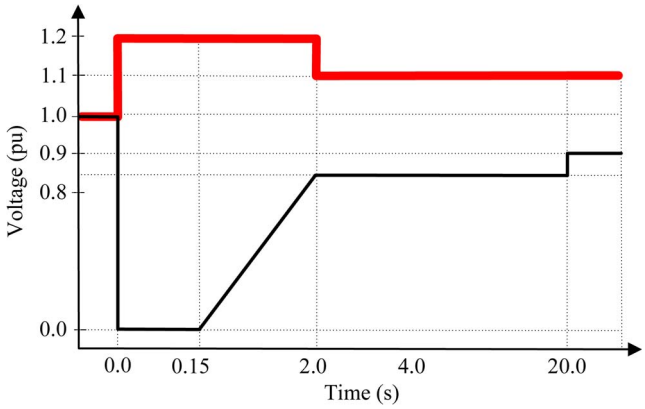

Fig. 2. LVRT specification for wind energy facilities [15].

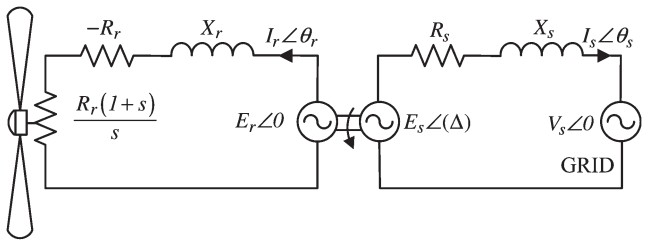

Fig. 3. Per-phase equivalent circuit of the SS-PMG.

between 47 and 52 Hz at a rate of change of 0.5 Hz/s. There are also several harmonic components present in the grid voltage, which could influence the dynamic behavior of the SS-PMG.

IV. Modeling of the SS-PMG

Due to the SS-PMG consisting of two electromagnetically separated generating units, it can be also modeled as two independent decoupled machines. A per-phase equivalent circuit is shown in Fig. 3. The rotor winding is short-circuited and is mechanically connected to the turbine, and the stator terminals are connected to the grid. A voltage is induced in the stator windings at grid frequency in the steady state, and in the short-circuited slip rotor, a voltage is induced at slip frequency. In this circuit, the slip rotor is referred to the grid frequency, and the slip speed is taken as positive in the generator mode. The modeling of the generator is done in the d-q reference frame that is fixed to the PM rotor, for both the grid-frequency and slip-frequency generator components.

A. Modeling Equations

The d-q equivalent circuits of the slip PMG and the PMSG are shown in Fig. 4. Note that a positive current is taken as flowing out of the machine. Hence, the d-q dynamic equations of the slip PMG and the PMSG fixed to the PM rotor are given, respectively, by

$$\begin{aligned} 0 &= -R_r i_{qr} - L_{qr}\frac{di_{qr}}{dt} - \omega_{\rm sle} L_{dr} i_{dr} + \omega_{\rm sle}\lambda_{mr} \\ 0 &= -R_r i_{dr} - L_{dr}\frac{di_{dr}}{dt} + \omega_{\rm sle} L_{qr} i_{qr} \end{aligned} \tag{1}$$

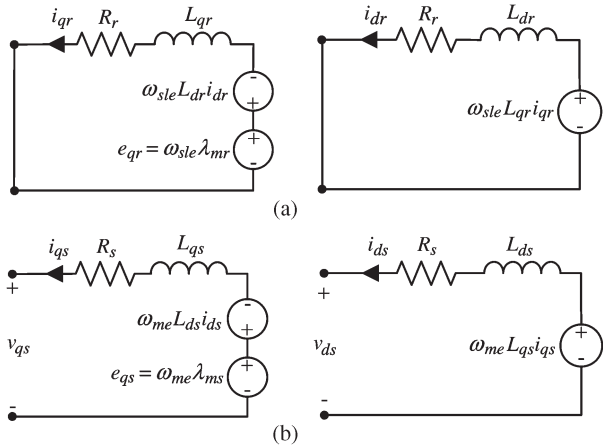

Fig. 4. D-Q equivalent circuits of (a) short-circuited slip PMG and (b) grid-connected PMSG.

$$\begin{aligned} v_{qs} &= -R_s i_{qs} - L_{qs}\frac{di_{qs}}{dt} - \omega_{me} L_{ds} i_{ds} + \omega_{me}\lambda_{ms} \\ v_{ds} &= -R_s i_{ds} - L_{ds}\frac{di_{ds}}{dt} + \omega_{me} L_{qs} i_{qs} \end{aligned} \tag{2}$$

where $\omega_{\rm sle}$ is the electrical slip speed equal to $\omega_{\rm sle} = p/2(\omega_t - \omega_m)$, and ω_t and ω_m are the turbine and PM rotor angular velocities, respectively [see Fig. 1(a)]. Subscripts r, s, and e refer to the slip PMG rotor, the PMSG stator, and the electrical speed, respectively. Hence, (L_{qr}, L_{dr}) and (L_{qs}, L_{ds}) are the d-q inductances of the slip PMG and the PMSG, respectively, and the flux linkages due to the PMs are indicated by λ_{mr} and λ_{ms}, respectively. The d-q inductances of the slip PMG and the PMSG are determined in general by

$$L_q = \frac{\lambda_q}{-I_q} + L_e \quad L_d = \frac{\lambda_d - \lambda_m}{-I_d} + L_e. \tag{3}$$

For inductance calculations, it is important that the end effects in the PMs and the end-winding inductance, i.e., L_e in (3), are taken into account. L_e is calculated using the methods presented in [21]. For accurate simulation, the d-q inductances are obtained from a 2-D or 3-D finite-element (FE) analysis. Although these inductances are shown to vary during different load conditions caused by saturation and cross-coupling effects, they are taken as constant to simplify the dynamic modeling.

The torque generated by the slip PMG and that by the PMSG are given, respectively, by

$$\tau_r = \frac{3}{4} p\left[(L_{qr} - L_{dr}) i_{dr} i_{qr} + \lambda_{mr} i_{qr}\right] \tag{4}$$

$$\tau_s = \frac{3}{4} p\left[(L_{qs} - L_{ds}) i_{ds} i_{qs} + \lambda_{ms} i_{qs}\right]. \tag{5}$$

The dynamics of the turbine (plus the slip rotor) and the PM rotor are expressed by

$$\tau_t - \tau_r - b_r\omega_t = J_t\frac{d\omega_t}{dt} \tag{6}$$

$$\tau_m = \tau_r - \tau_s - b_s\omega_m = J_m\frac{d\omega_m}{dt} \tag{7}$$

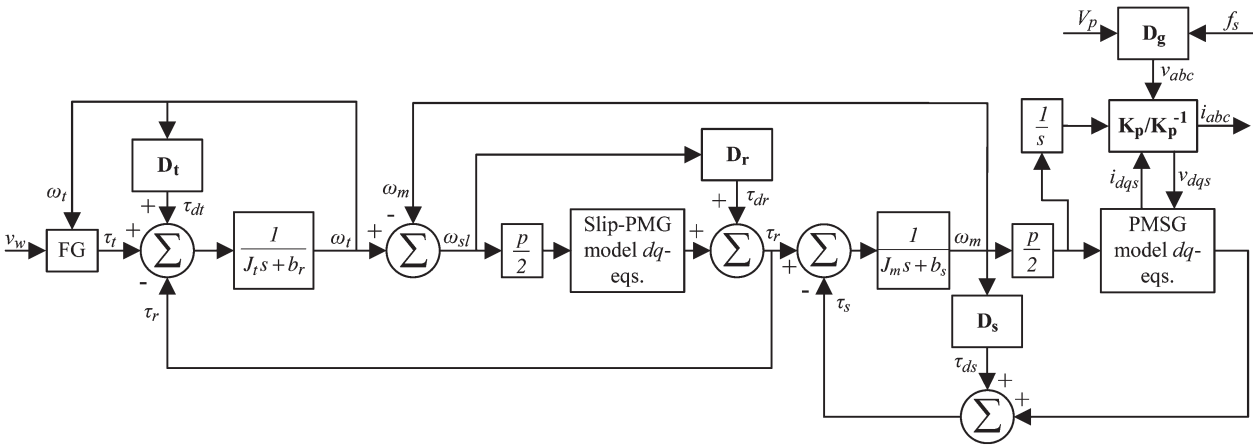

Fig. 5. Top-level transfer function of the grid- and turbine-connected SS-PMG wind energy system.

where τ_t is the torque generated by the turbine, τ_m is the resultant torque acting on the PM rotor, and J_t and J_m are the inertia of the turbine (plus the slip rotor) and the PM rotor, respectively, as shown in Fig. 1(a). The friction coefficients are indicated by b_r and b_s for the slip PMG and PMSG units, respectively.

B. Modeling Implementation

From the given mathematical equations, a complete transfer function simulation model of a single grid-connected SS-PMG wind energy system is obtained, as shown in Fig. 5. The simulation model is implemented in Matlab Simulink. The input parameters of the system are wind speed v_w and grid voltages v_{abc} at a certain frequency f_s, where V_p is the peak voltage value. The function generator in Fig. 5 gives the torque–speed curves of the turbine versus the wind speed and the rotational speed. Voltages v_{abc} are transformed to v_{dqs} using the Park transformation $\mathbf{K_p}$. In Fig. 5, the outputs are grid currents i_{abc}, which are calculated using the inverse Park transform $\mathbf{K_p^{-1}}$.

The disturbances, as discussed in Section III, are injected into the system from three main sources: 1) the turbine disturbances, e.g., from tower shadowing, tower oscillations, and turbine shear, which are indicated by the block function $\mathbf{D_t}$ in Fig. 5; 2) the torque ripple disturbances caused by the interaction between the slip rotor and the stator with the common PM rotor, which are indicated by $\mathbf{D_r}$ and $\mathbf{D_s}$, respectively, in Fig. 5; and 3) the grid voltage disturbances such as frequency variations, amplitude variations, and harmonics, which are indicated by $\mathbf{D_g}$. The turbine-disturbance torque signal is indicated by τ_{dt}, and the torque ripple by τ_{dr} and τ_{ds} for the slip PMG and the PMSG, respectively. Furthermore, these disturbance signals are dependent on ω_t, $\omega_{\rm sl}$, and ω_m. Thus, to determine the disturbance signal to be injected into the system, an amplitude and harmonic order n needs to be specified, which is coupled to a disturbance function. The amplitudes of the turbine, slip PMG, and PMSG torque disturbances are indicated by T_{dt}, T_{dr}, and T_{ds}, respectively. For the torque ripple disturbances, the amplitude and the harmonic order of the torque ripple waveform are determined from the FE analysis. Fig. 6 shows

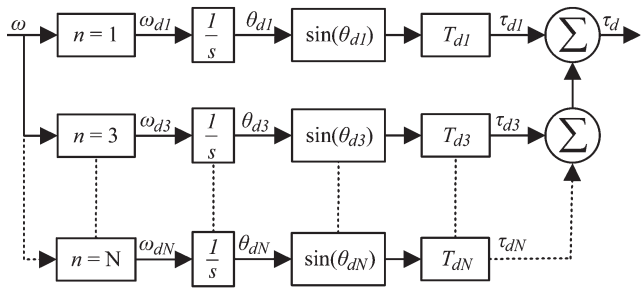

Fig. 6. General modeling for each torque disturbance function, namely, $\mathbf{D_t}$, $\mathbf{D_r}$, and $\mathbf{D_s}$ in Fig. 5.

Fig. 7. Case-study 15-kW SS-PMG, with a nonoverlap SL winding PMSG unit and a nonoverlap DL winding slip PMG unit, being field tested.

the modeling of the disturbance functions as done for $\mathbf{D_t}$, $\mathbf{D_r}$, and $\mathbf{D_s}$ in Fig. 5. The input is the relevant angular speed that is multiplied with the harmonic order n of the disturbance. First, ω_{dn} is integrated to obtain the position θ_{dn} where the sinus value is obtained and then multiplied by the harmonic disturbance amplitude T_{dN} of the specific signal.

V. Case Study SS-PMG

The turbine and SS-PMG parameters for a 15-kW wind turbine system, as shown in Fig. 7 and as used in this paper, are given in Table I. For the PMSG, a nonoverlap single-layer (SL) winding is used due to the easy manufacturing of this machine, as shown in Fig. 8(a). For the slip PMG, a nonoverlap

TABLE I
EVALUATED PARAMETERS OF THE WIND TURBINE SYSTEM

Parameter	Value	Parameter	Value
V_s	230 V	poles	40
I_s	23 A	I_r	9.2 kA
f_s	50 Hz	Rated slip	3 %
R_s	0.39 Ω	R_r	5.87 μΩ
L_{ds}	8.4 mH	L_{dr}	101.77 nH
L_{qs}	10.3 mH	L_{qr}	137.61 nH
L_{es}	2.9 mH	L_{er}	32.88 nH
λ_{ms}	1.04 Wb.t	λ_{mr}	3.62 mWb.t
J_m	8 kg.m^2	J_t	330 kg.m^2
Swept diameter	7.2 m	n_t	150 r/min
Rated power, P_s	15 kW	Rated torque, T_t	1000 Nm

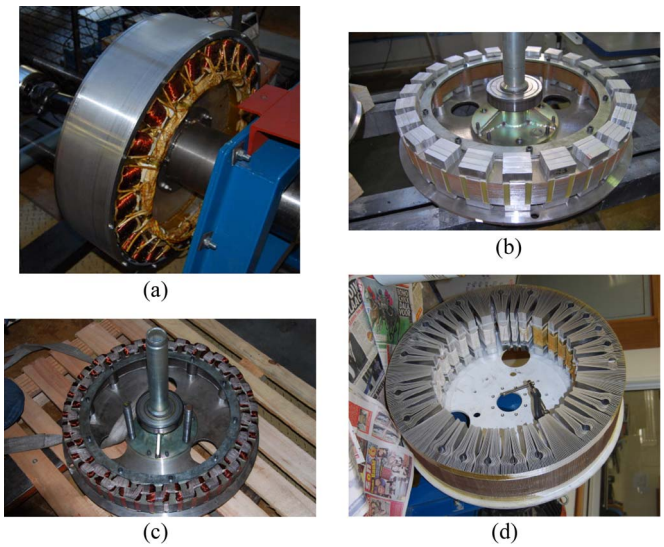

Fig. 8. (a) SL PMSG, (b) SL slip PMG, (c) DL slip PMG, and (d) brushless-dc slip PMG prototypes.

double-layer (DL) winding is used, as shown in Fig. 8(c). In [14], the nonoverlap winding has the advantage of much easier construction and a lower torque ripple, as opposed to conventional overlap cage windings, although it has a higher mass and PM content. There are also other slip PMG topologies that are evaluated, such as a nonoverlap SL slip PMG, as shown in Fig. 8(b), and a novel brushless-dc slip PMG topology, as in [14] and as shown in Fig. 8(d). These different slip PMGs have different torque ripple properties, which gives a better indication of the dynamic effects of the torque ripple on the SS-PMG wind turbine system.

VI. SIMULATION RESULTS

For the dynamic simulations, the prototype SS-PMG, with parameters as given in Table I, is used. Some of the machine parameters in Table I are also varied in order to gain a better understanding of the effect of each of these parameters on the stability of the system.

A. Transient Turbine Torque Conditions

The transient turbine torque conditions refer to the torque response of the SS-PMG due to changes in wind speed and due to turbine disturbances, as discussed in Section III.

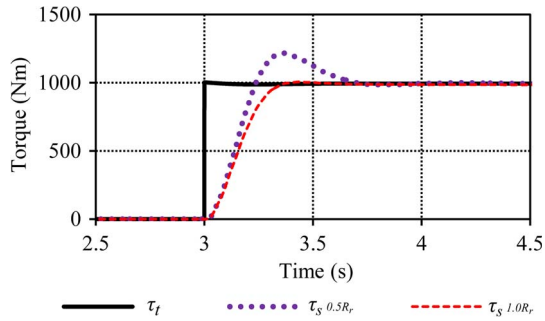

Fig. 9. Simulated torque response for a rated wind speed (11 m/s) step input for $0.5 \times R_r$ and $1 \times R_r$ for the SS-PMG.

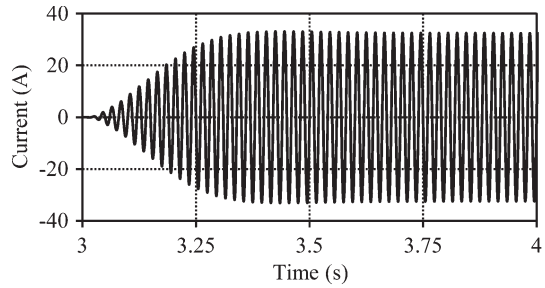

Fig. 10. Simulated stator current response for a rated wind speed (11 m/s) step input for $1 \times R_r$ for the SS-PMG.

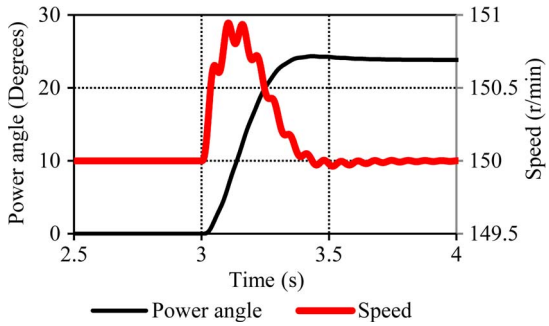

Fig. 11. Simulated stator power angle and the PM rotor speed response for a rated wind speed (11 m/s) input for $1 \times R_r$ for the SS-PMG.

In Fig. 9, the transient response of the stator counter torque τ_s is shown for a turbine torque input step from 0 to the rated torque at $\tau_t = 1000$ N · m. The corresponding stator grid current response is shown in Fig. 10, and the power angle and the PM rotor speed response are shown in Fig. 11. Such a severe torque step will seldom occur in a real application, but this gives an adequate indication to the stability of the system regarding turbine torque changes. For this severe torque step, a very stable overdamped response is observed for the case-study SS-PMG.

The same simulation is repeated for a change in the internal resistance of the slip PMG R_r by reducing it by about 50%, which can typically occur if the conducting material of the slip PMG is changed from aluminum to copper. This will decrease the rated slip by the same amount from 3% to 1.5%. A clear overshoot is observed in Fig. 9, in this case for the slip PMG. As explained in [4], the rated slip coincides with the rated efficiency of the machine; thus, a lower slip value leads to higher efficiency but less stability. Moreover, what is important in this case is the inductance value of the PMSG stator. It

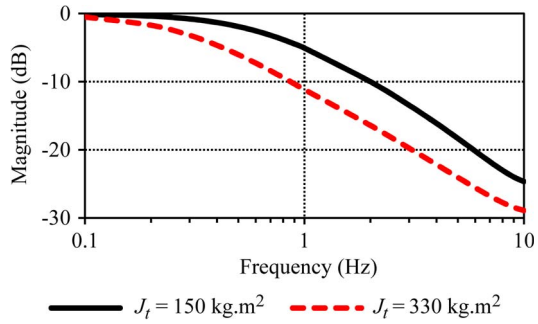

Fig. 12. Frequency response of $\Delta\tau_s/\tau_{dt}$ for $J_t = 150\ \text{kg} \cdot \text{m}^2$ (laboratory test setup) and the $J_t = 330\ \text{kg} \cdot \text{m}^2$ (7.2-m turbine) of the SS-PMG system.

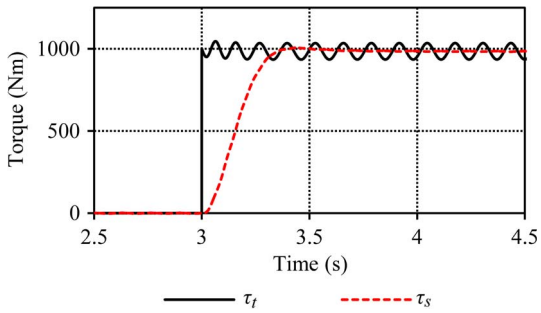

Fig. 13. Simulated torque τ_s response of the SS-PMG system for a 7.5-Hz disturbance in turbine torque τ_t (typical tower shadow effect).

is found that, if the stator inductance is decreased by more than 50% of the given value for the nonoverlap SL winding machine, the system becomes unstable for this transient torque step input. This reduction in inductance can typically occur if a nonoverlap DL PMSG or a conventional overlap winding PMSG is used for the grid-connected stator. By changing the resistance, inductance, and inertia of the common PM rotor, the electrical and mechanical time constants are influenced, which in turn dictates the damping ratio of the system.

In Fig. 12, the bandwidth of the system is shown with τ_t as the input and τ_s as the output. The frequency response is shown for the values of the turbine and the slip PMG inertia, with $J_t = 330\ \text{kg} \cdot \text{m}^2$ corresponding to the turbine system with a swept diameter of 7.2 m and with $J_t = 150\ \text{kg} \cdot \text{m}^2$ corresponding to the laboratory test setup, which includes the inertia of the driving machine and the gearbox. For the laboratory test system, a bandwidth of just below 1 Hz is observed, and for the turbine system, a bandwidth of about 0.3 Hz is observed. Typical disturbances, as discussed in Section III, will generate the turbine torque pulsation frequencies of nf_t, with $n = 1$ and $n = 3$. For all practical purposes, the speed of the turbine can be taken as constant with a maximum variation of only 3%, which corresponds to the rated slip. Thus, at the rated turbine speed of 150 r/min, $f_t = 2.5$ Hz. It is clearly shown in Fig. 12 that all the disturbances with a frequency of 2.5 Hz and higher are well above the cutoff frequency of the system. This explains the zero torque output response in Fig. 13 for a turbine-disturbance torque input of 7.5 Hz that is typically caused by the tower shadowing effect. This is a significant result for the proposed fixed-speed SS-PMG wind turbine system as possible voltage flickering on the grid due to tower shadowing, wind shear, tower oscillation, and yaw error will not occur.

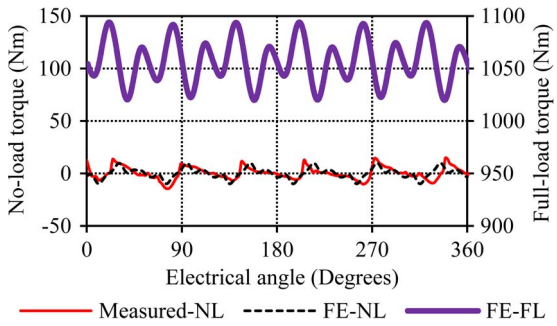

Fig. 14. FE-predicted NL and FL torque ripple, and the measured NL torque ripple versus the electrical angle for the SL slip PMG.

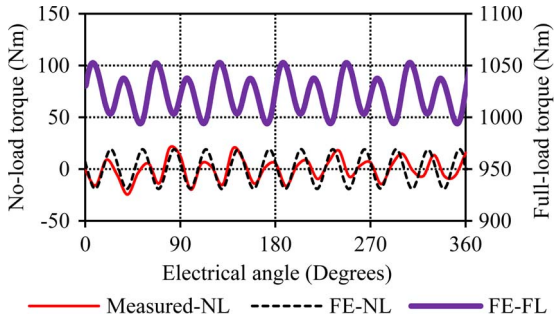

Fig. 15. FE-predicted NL and FL torque ripple, and the measured NL torque ripple versus the electrical angle for the DL slip PMG.

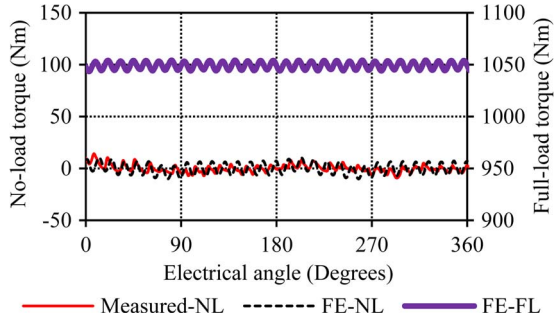

Fig. 16. FE-predicted NL and FL torque ripple, and the measured NL torque ripple versus the electrical angle for the brushless-dc slip PMG.

B. Generator Torque Disturbances

Internal generator disturbances refer to the torque ripple interaction between the slip PMG plus the PMSG stator and the common PM rotor, and these are modeled in Figs. 5 and 6. Due to the much smaller inertia of the common PM rotor, the bandwidth is much higher. This could be problematic particularly because the torque ripple frequency of the slip PMG is very low due to the fact that the slip PMG operates at slip frequency. Figs. 14–16 show the torque ripple characteristics of the nonoverlap SL and DL winding slip PMGs, and the brushless-dc slip PMG, respectively. The no-load (NL) cogging torque and the full-load (FL) torque ripple are shown in each of the cases. Clearly, it is necessary to evaluate a large spectrum of torque ripple characteristics. With slip frequency f_{sl} equal to sf_s, the torque ripple frequency for the slip PMG is calculated as nf_{sl}, where n is the harmonic order. For the slip PMG, the

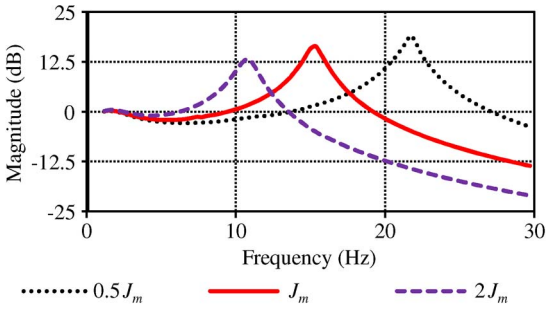

Fig. 17. Frequency response of $\Delta\tau_s/\Delta\tau_{dr}$ for the inertia of the PM rotor equal to the $J_m \times 0.5$, $J_m \times 1.0$, and $J_m \times 2$ of the SS-PMG system.

torque ripple frequency will vary with the slip. In Figs. 14–16, the main harmonics identified are at $n = 1$, 6, 12, and 30. Differences are also observed in some cases for n between the FL torque ripple and the NL cogging torque. Furthermore, in most cases, the FL torque ripple is higher than the NL cogging torque, particularly for the nonoverlap SL slip PMG. The torque ripple frequency for the PMSG is fixed as the common PM rotor rotates at a fixed speed. It is found that, due to the very high frequency of this ripple component with $nf_s = 300$ Hz for $n = 6$, and $f_s = 50$ Hz, it has no effect on the dynamic performance of the system.

Fig. 17 shows the bandwidth of the torque ripple disturbance input for $\Delta\tau_s/\Delta\tau_{dr}$, where $\Delta\tau_s$ is the ripple component in the PMSG torque response. The bandwidth is shown for the different values of the PM rotor inertia. A clear resonance value is observed in all three cases, with the frequency value at which this resonance occurs dependent on the size of J_m. For the case study system, a resonance is observed at about 15 Hz. The rated slip of the system and the value of the harmonic order n for the torque ripple waveform will determine if this resonance area falls within the operating region of the slip PMG. However, although the operating range of the slip PMG is below the resonance area, the torque ripple disturbance is still transferred to the grid current at $\Delta\tau_s/\Delta\tau_{dr} = 1$.

From the observed torque ripple characteristics, it is clear that the low-frequency torque ripple of the slip PMG is passed through the system to the grid current over the whole load range of the SS-PMG. Although it is not found to dynamically destabilize the system in any way, it could cause flickering effects on the grid if the unwanted disturbance frequency is in the range where flickering is a concern. Thus, it is essential that the torque ripple is minimized to the lowest possible value in the design optimization of the slip PMG.

C. Grid Voltage Disturbances

The disturbances from the grid relates to the variations in the voltage and frequency, as discussed in Section III. Fig. 18 shows the effect on stator torque τ_s and PM rotor speed ω_m when a 2% fifth-order harmonic is added to the voltage waveform. This leads to a high-frequency oscillation in τ_s, which is not transferred to the rest of the system, as can be seen in the PM rotor speed in Fig. 18. Fig. 19 shows the effect of varying the frequency between 47 and 52 Hz at a rate of 0.5 Hz/s, as specified in [15], on τ_s and on ω_m. No oscillatory behavior is observed.

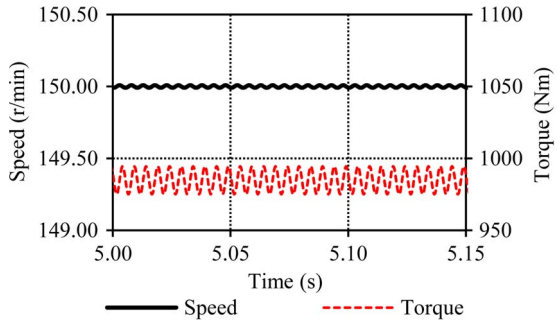

Fig. 18. Simulated PM rotor speed and the stator counter torque response for a 2% fifth-order harmonic in the voltage waveform at rated power for the SS-PMG.

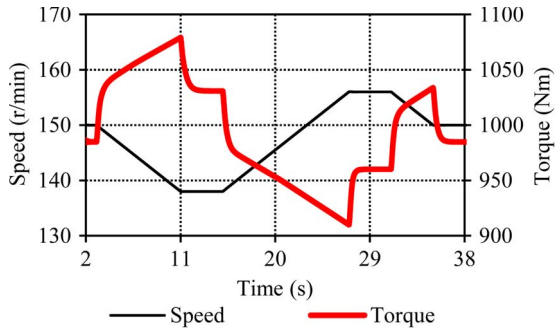

Fig. 19. Simulated PM rotor speed and the stator counter torque response for a variation in grid frequency for $47 \leq f_s \leq 52$ Hz at a rate of change of 0.5 Hz/s at rated power for the SS-PMG.

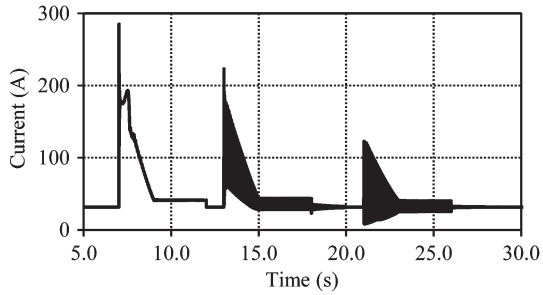

Fig. 20. Simulated peak stator current response for three-phase, two-phase and single-phase grid faults, as shown from left to right, at rated power for the SS-PMG with the inductance values reduced by 45%.

For the LVRT analysis of the system, the voltage specification given in Fig. 2 is used. The aim of this paper is only to determine if the SS-PMG is stable under transient grid voltage conditions and not to evaluate the techniques to limit the short-circuit current, as done in [10]. For a three-phase fault condition, it was found that the case-study SS-PMG with a nonoverlap SL winding [see Fig. 8(a)] could not handle the three-phase fault, and the system became unstable. This is because the value of power angle Δ exceeds 180° as the peak torque that the generator is capable of is not sufficient to keep the generator in synchronism, and pole slipping occurs. Pole slipping is mentioned as undesirable in [2]. However, it does not matter if the generator is pulled back into synchronism and the system becomes stable again. In this case, the d-q inductances of the PMSG unit are reduced by a factor of $0.55 \times (L_{ds},\ L_{qs})$. This is typically the case if the nonoverlap SL winding is replaced by a nonoverlap DL winding. This

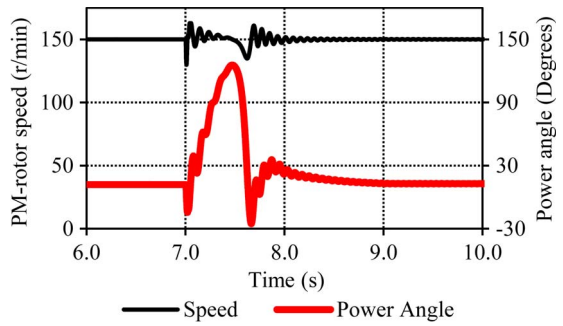

Fig. 21. Simulated PM rotor speed and the power angle response for a three-phase grid fault at rated power for the SS-PMG with the inductance values reduced by 45%.

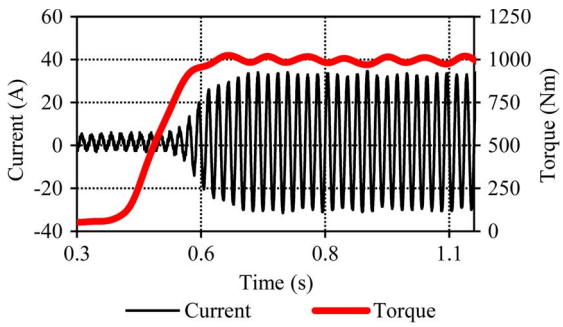

Fig. 22. Measured stator current response and the input torque for a step input from 0 to 1000 N · m for the brushless-dc slip PMG used in the SS-PMG.

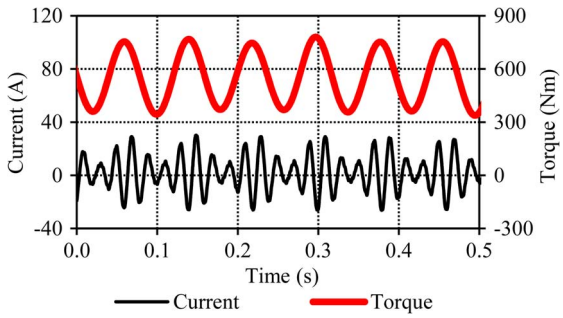

Fig. 23. Measured instantaneous stator current and torque at partial load and resonance frequency, with the SL slip PMG used in the SS-PMG.

reduction in inductance, however, means that the peak fault current increases significantly. From left to right in Fig. 20, the peak current response is shown for the three-phase, two-phase, and single-phase grid faults for the SL PMSG unit, with its inductance modified. The three-phase fault is clearly shown to be the most severe for the SS-PMG. Fig. 21 shows the responses of ω_m and Δ to the three-phase fault.

VII. Measurements

For the laboratory testing of the SS-PMG, it is connected through a gearbox to the drive motor that is controlled by a variable frequency drive. Fig. 22 shows a step input in the torque and the resulting stator grid current response corresponding to the simulated turbine torque input step in Fig. 9. It should be noted that the torque sensor is placed between the inertial components of the gearbox and the slip rotor. With the inertia of the gearbox much larger than that of the slip rotor, the resulting measurement will reflect the torque interaction

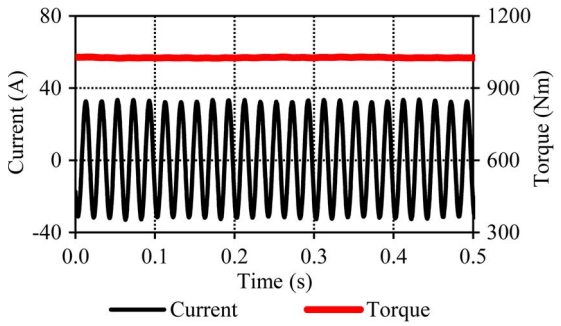

Fig. 24. Measured instantaneous stator current and torque at FL for the brushless-dc slip PMG SS-PMG.

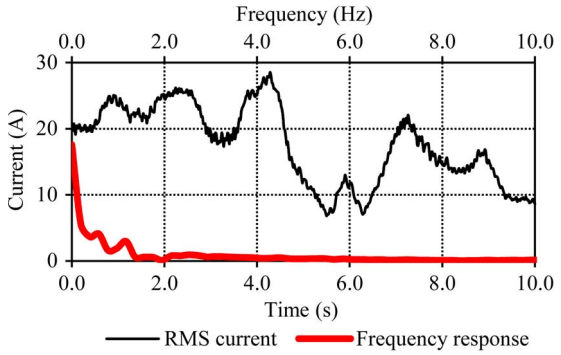

Fig. 25. Measured RMS grid current and the RMS current oscillation frequency content for the case-study 15-kW SS-PMG, as in Fig. 7, with a nonoverlap SL winding PMSG unit and a nonoverlap DL winding slip PMG unit, during field testing to obtain the bandwidth of the system, as in Fig. 12.

between the slip rotor and the common PM rotor. Due to the large gearbox inertia, the torque input step is done on a different test bench with a smaller driving motor and gearbox, as such a small step time could not be realized on the larger test bench used for the other measurements. However, it is found that the couplings used on the smaller test bench causes several unwanted dynamic effects, which explains the observed ripple component in the input torque in Fig. 22.

Fig. 23 shows the measured input torque and the output grid current at a load of about 0.6 p.u. using the nonoverlap SL slip PMG. At this load point, the torque ripple frequency is within the resonance area, as shown in Fig. 17. The results are a severe oscillation in the torque and a high distortion in the grid current. These effects are clearly undesirable in a grid-connected wind turbine system. In Fig. 24, the measured torque and grid current for the brushless-dc slip PMG are shown at a rated load. In this case, the torque ripple frequency corresponds to a value higher than that of the resonance area, and very little distortion of the grid current is observed. Furthermore, no dynamic effects from the test bench are observed as is the case for the smaller test bench in Fig. 22. Fig. 25 shows the measured RMS grid current and the oscillation frequency content in the RMS current for the SS-PMG during the field testing for a 10-s window. Although the wind site is not optimal due to the very high turbulence intensity, as clearly shown in Fig. 25, it gives a very good indication of the stability of the SS-PMG. Furthermore, in the oscillation frequency content of the measured RMS grid current, it is clearly shown that only the very low-frequency components are transferred to the grid, as predicted in Fig. 12.

VIII. Conclusion

The transfer function model that is developed for the SS-PMG in this paper has been shown to give a good indication of the dynamic characteristics of the system. From the simulated and measured responses of the case-study 15-kW SS-PMG system, it is shown that the system remains stable even for large step inputs in the turbine torque. Interesting findings include the effects of the per-phase resistance of the slip PMG and the inductance of the PMSG on the stability of the SS-PMG. It is found that, when replacing the aluminum winding of the slip rotor with copper, the damping ratio of the system is clearly reduced. Furthermore, it is found that the SS-PMG wind generator system has a very low bandwidth (< 1 Hz). This causes the system to act as a filter against turbine torque pulsations caused by tower shadowing, wind shear, and tower oscillation, preventing voltage flickering from occurring, which is a huge advantage. A problematic dynamic disturbance is the torque ripple of the slip PMG. The high-frequency torque ripple of the PMSG is shown to be filtered out and is not a factor. It is shown that the torque ripple of the low-frequency slip PMG is passed to the grid current over the entire load range. Thus, it is essential that the torque ripple of the slip PMG should be minimized to the lowest possible value in the design optimization. The torque ripple, however, is shown to not destabilize the dynamic operation of the SS-PMG in any way. It is furthermore shown that the SS-PMG is sensitive to grid voltage changes. Grid harmonic voltages are shown to cause the harmonic currents of the same order to flow in the PMSG unit, but they do not influence the dynamic operation of the rest of the system. The response of the SS-PMG to grid faults is shown to largely depend on the inductance value of the PMSG unit. During low-voltage conditions, the directly grid-connected PMSG supports the grid voltage using the reactive current, which is much higher than the reactive current support that is provided by other wind generator topologies.

References

[1] A. Westlake, J. Bumby, and E. Spooner, "Damping the power-angle oscillations of a permanent−magnet synchronous—generator with particular reference to wind turbine applications," *IEE Proc. Elect. Power Appl.*, vol. 143, no. 3, pp. 269–280, May 1996.

[2] H. Müller, M. Pöller, A. Basteck, M. Tilshcher, and J. Pfister, "Grid compatibility of variable speed wind turbines with directly coupled synchronous generator and hydro−dynamically controlled gearbox," in *Proc. 6th Int. Workshop Large Scale Integr. Wind Power Transmiss. Netw. Offshore Wind Farms*, 2006, pp. 307–315.

[3] S. Grabic, N. Celanovic, and V. Katic, "Permanent magnet synchronous generator cascade for wind turbine application," *IEEE Trans. Power Electron.*, vol. 23, no. 3, pp. 1136–1142, May 2008.

[4] J. H. J. Potgieter and M. J. Kamper, "Design of new concept gearless direct−grid connected slip−synchronous permanent magnet wind generator," *IEEE Trans. Ind. Appl.*, vol. 48, no. 3, pp. 913–922, May/Jun. 2012.

[5] F. Punga and L. Schon, "Der neue kollektorlose Einphasenmotor der Firma Krupp," *Elektrotech. Zeitschrift*, vol. 47, no. 29, pp. 877–881, 1926.

[6] B. Hagenkort, T. Hartkopf, A. Binder, and S. Jöckel, "Modelling a direct drive permanent magnet induction machine," in *Proc. ICEM*, 2000, pp. 1495–1499.

[7] E. Tröster, M. Sperling, and T. Hartkopf, "Finite element analysis of a permanent magnet induction machine," in *Proc. Int. SPEEDAM*, 2006, pp. 179–184.

[8] A. Thomas, "A doubly-fed permanent magnet generator for wind turbines," M.S. thesis, Dept. Elect. Eng. Comput. Sci., Massachusetts Inst. Technol., Cambridge, MA, USA, 2004.

[9] U. Hoffmann, P. Bouwer, and M. J. Kamper, "Direct grid connection of a slip−permanent magnet wind turbine generator," in *Proc. ECCE*, Phoenix, AZ, USA, 2011, pp. 2373–2380.

[10] U. Hoffmann and M. J. Kamper, "Low voltage ride−through compensation for a slip−permanent magnet wind turbine generator," in *Proc. 20th SAUPEC*, Cape Town, South Africa, 2011, pp. 191–196.

[11] A. T. Spies and M. J. Kamper, "Reactive power control of a direct grid connected slip synchronous permanent magnet wind generator," in *Proc. IEEE ICIT*, Cape Town, South Africa, 2013, pp. 770–775.

[12] J. H. J. Potgieter and M. J. Kamper, "Design specifications and optimisation of a directly grid−connected PM wind generator," in *Proc. ECCE*, Denver, CO, USA, 2013, pp. 882–889.

[13] R. Vermaak, J. H. J. Potgieter, and M. J. Kamper, "Grid−connected VSC−HVDC wind farm system and control using permanent magnet induction generators," in *Proc. IEEE Int. Conf. PEDS*, 2009, pp. 897–902.

[14] J. H. J. Potgieter and M. J. Kamper, "Optimum design and technology evaluation of slip permanent magnet generators for wind energy applications," in *Proc. IEEE ECCE*, Raleigh, NC, USA, 2012, pp. 2342–2349.

[15] Grid code requirements for wind energy facilities connected to distribution or transmission systems in South Africa, Jul. 2012, Version 5.4.

[16] J. Gutierrez, J. Ruiz, P. Saiz, I. Azcarate, L. A. Leturiondo, and A. Lazkano, "Power quality in grid-connected wind turbines," in *Proc. Wind Turbines*, 2011, pp. 547–570.

[17] T. Thiringer and J. Dahlberg, "Periodic pulsations from a three-bladed wind turbine," *IEEE Trans. Energy Convers.*, vol. 16, no. 2, pp. 128–133, Jun. 2001.

[18] D. S. L. Dolan and P. W. Lehn, "Simulation model of wind turbine 3p torque oscillations due to wind shear and tower shadow," *IEEE Trans. Energy Convers.*, vol. 21, no. 3, pp. 717–724, Sep. 2006.

[19] M. Pöller and S. Achilles, "Aggregated wind park models for analyzing power system dynamics," in *Proc. 4th Int. Workshop Large-scale Integr. Wind Power Transmiss. Netw. Offshore Wind Farms*, Billund, Denmark, 2003, pp. 1–10.

[20] J. Sopanen, V. Ruuskanen, J. Nerg, and J. Pyrhönen, "Dynamic torque analysis of a wind turbine drive train including a direct-driven permanent magnet generator," *IEEE Trans. Ind. Electron.*, vol. 58, no. 9, pp. 3859–3867, Sep. 2011.

[21] J. H. J. Potgieter and M. J. Kamper, "Evaluation of calculation methods and the effects of end−winding inductances on the performance of non−overlap winding PM machines," in *Proc. Int. Conf. Electr. Mach.*, Marseille, France, 2012, pp. 243–249.

Johannes H. J. Potgieter (S'10) was born in Oudtshoorn, South Africa, in 1985. He received the B.Eng. and M.Sc. (Eng.) degrees in electrical and electronic engineering from the University of Stellenbosch, Stellenbosch, South Africa, in 2008 and 2011, respectively, where he is currently working toward the Ph.D. (Eng.) degree in the Department of Electrical and Electronic Engineering.

His current research interests include wind power generation solutions and the optimization of permanent-magnet machine technologies, including computer-aided design.

Maarten J. Kamper (SM'08) received the M.Sc. (Eng.) and Ph.D. (Eng.) degrees from the University of Stellenbosch, Stellenbosch, South Africa, in 1987 and 1996, respectively.

Since 1989, he has been with the Department of Electrical and Electronic Engineering, University of Stellenbosch, where he is currently a Professor of electrical machines and drives. His research interests include computer-aided design and control of reluctance, and permanent-magnet and induction-machine drives.

Prof. Kamper is a Scientist supported by the South African National Research Foundation and a Registered Professional Engineer in South Africa.